Development of a Polarized Helium-3 Ion Source for RHIC using the Electron Beam Ion Source

by

Charles Samuel Epstein

Submitted to the Department of Physics
in partial fulfillment of the requirements for the degree of

Bachelor of Science

at the

MASSACHUSETTS INSTITUTE OF TECHNOLOGY

June 2013

Author .....
Department of Physics
May 10, 2013

Certified by .....
Professor Richard G. Milner
Professor of Physics, Director of Laboratory for Nuclear Science
Thesis Supervisor

Accepted by .....
Professor Nergis Mavalvala
Senior Thesis Coordinator, Department of Physics

Development of a Polarized Helium-3 Ion Source for RHIC using the Electron Beam Ion Source

by

Charles Samuel Epstein

Submitted to the Department of Physics
on May 10, 2013, in partial fulfillment of the
requirements for the degree of
Bachelor of Science

Abstract

This thesis presents my work on the design and development of a source of polarized Helium-3 ions for the Relativistic Heavy Ion Collider at Brookhaven National Lab, Upton, NY. The ^{3}He atoms will be polarized using the technique of metastability-exchange optical pumping (MEOP), and will then be flowed into the newly commissioned Electron Beam Ion Source (EBIS). Fully stripped $^3He^{++}$ ions will be extracted and their polarizations measured at low energies before acceleration in the RHIC complex.

Thesis Supervisor: Professor Richard G. Milner
Title: Professor of Physics, Director of Laboratory for Nuclear Science

Acknowledgments

I wish to express my gratitude to all of the people who have made this project possible. At MIT, our collaborators are Richard Milner, James Maxwell, and Eliza Mace; at Brookhaven National Laboratory, Jim Alessi, Ed Beebe, Alexander "Sasha" Pikin, Thomas Roser, Wolfram Fischer, Xaofeng Gu, and Anatoli Zelenski. We have had very helpful discussions with Werner Heil, Sergei Karpuk, and Ernst Otten (U. Mainz), Pierre-Jean Nacher (ENS, Paris), and Guilhem Collier (University of Cracow, Poland). Sasha's advice has been vital in our understanding of the EBIS device and magnetic field, and he has provided us with many drawings, much data, and code. Thank you also to Daniel Kleppner for discussions that have been extremely helpful towards understanding the atomic processes inside EBIS.

The engineers at Bates, under the leadership of Jim Kelsey, have been invaluable, and thank you especially to Ernie Ihloff who has met with me many times about this project and from whom I've learned a great deal. Brian O'Rourke has played a key role in making the new sealed cells. Thanks also to Genya Tsentalovich for helping us learn how to use the VectorFields Tosca/Opera electromagnetic modeling software.

Once again, a most important thanks to Richard Milner for being an amazing mentor and for giving me so many extraordinary opportunities. I'm looking forward to returning as a grad student in the fall.

Contents

List of Figures

Chapter 1

Physics Motivation

1.1 Introduction

An issue in nuclear physics currently receiving much attention is that of the spin structure of the nucleon. Experiments at SLAC, CERN, and DESY, have determined that quarks only contribute about 25% of the nucleon's spin. As a result, current experiments such as those at RHIC-spin are testing the contributions of gluons in order to determine how the remaining 75% of the spin arises. A useful tool in all of these studies has been the spin-polarized proton. However, it is beneficial to perform experiments with both isospin configurations of the nucleon as both a control and a place to search for new physics. According to current theoretical predictions, the polarized neutron provides a similar gluon distribution to that of the proton, but with a different configuration of quarks. A polarized neutron beam at RHIC-spin would thus be a remarkable asset to the study of nucleon spin structure. [8]

Due to the difficulties associated with manipulating free neutrons, experiments studying the polarized neutron have often used polarized deuterons or ^{3}He. However, the deuteron is not suitable for beam formation because of its low magnetic moment, which makes spin manipulation in accelerators difficult. The magnetic moment of ^{3}He is similar to that of the free neutron due to the pairing of the two protons in a low-energy shell with opposite spin states. This reasonable magnetic moment allows the spins to be manipulated in accelerators using standard technology such as siberian

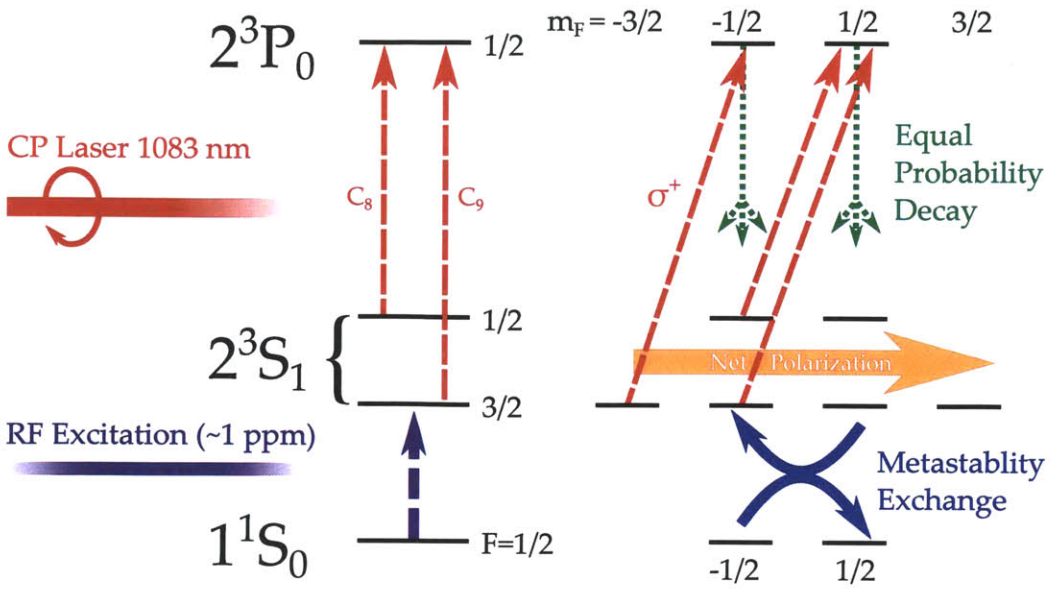

Figure 1-1: Diagram of the MEOP process. (J. Maxwell)

snakes. For these reasons, it is of great interest to develop a high-intensity source of highly polarized ^{3}He. [8]

Previous experiments have performed elastic scattering (BLAST at MIT-Bates South Hall Ring) or deep inelastic scattering (HERMES at HERA, DESY) using polarized electrons on a polarized ^{3}He internal gas target. Upgrading the ^{3}He to beam energies in a future electron-ion collider (eRHIC) would enable fundamental tests of theoretical predictions of the Standard Model, such as the Bjorken Sum Rule. Until then, a polarized ^{3}He ion source at RHIC would enable polarized np collisions from the onset, allowing new types of QCD studies to be performed and providing a means for other nucleon spin structure tests.

1.2 Polarization of ^{3}He

Low-energy sources of polarized $^3He^+$ ions have been developed several times in the past. A 50 particle nA, 65% polarized source was developed at the University of Birmingham, UK [2]. A collaboration between Rice University and Texas A&M developed an 8 particle μA, 11% polarized source [4]. At Laval University, Canada, a source polarized using a Stern Gerlach based method provided 100 particle nA at

95% polarization [13]. It is planned to provide a high-current, 500 particle nA source of 70% polarized $^3He^{++}$ ions to RHIC.

Metastability-exchange optical pumping (MEOP) is our method of choice to polarize the ^{3}He atoms. In this technique, a weak RF discharge excites atoms into the metastable 2^3S state, where they are pumped to the 2^3P states by 1083 nm circularly polarized laser light tuned to either the C_8 or C_9 transition (Fig. 1-1). This polarizes the optical electron, whose spin state couples to the nuclear state through the hyperfine interaction. Metastability exchange collisions then occur, in which atoms can swap electron configurations, allowing the nuclear polarization to propagate to the ground state atoms. MEOP has been performed with spectacular success. Modern ytterbium fiber lasers, replacing the dated Nd:YAG systems, have allowed highly-polarized, high-current MEOP systems to be constructed. At the University of Mainz, a flow rate of 8×10^{18} ^{3}He/sec at polarizations over 70% has been demonstrated [8].

1.2.1 MEOP Process

To illustrate the MEOP process, we consider a ground state atom with an electronic and nuclear states described by the density matrices ρ_{Ge} and ρ_{GN}, and a metastable atom with electronic state ρ_{Me} and nuclear state ρ_{MN}. The density matrices that characterize the ground state and metastable atoms are then $\rho_G = \rho_{Ge} \otimes \rho_{GN}$ and $\rho_M = \rho_{Me} \otimes \rho_{MN}$, respectively. After optical pumping polarizes the electronic state of the metastable atom, we consider the coupling of the nuclear and electronic spins via the hyperfine interaction, represented by the projection onto a hyperfine sublevel F: $\rho'_{MN} = \Sigma_F P_F \rho_{MN} P_F = \rho_{MN-\mathrm{Pol}}$ where P_F is the projection operator onto the respective F sublevel [3]. After coupling occurs, the density matrix becomes $\rho'_M = \rho'_{Me} \otimes \rho_{MN-\mathrm{Pol}}$. Following this, a metastability exchange collision occurs, transferring the polarization to a ground state atom. The density matrix of the ground state atom thus becomes $\rho''_G = \rho_{Ge} \otimes \rho_{MN-\mathrm{Pol}}$, and that of the metastable atom becomes $\rho''_M = \rho_{Me} \otimes \rho_{GN}$. This illustrates the electronic states being swapped. A summary of the process can be seen in Table 1.1. The result of the interaction is that a metastable atom is polarized electronically by optical pumping, and then transfers this electronic

angular momentum to its nucleus, which can then be transferred to a ground state atom, causing nuclear polarization of the ground state population.

Table 1.1: An overview of the MEOP process, based on table by [3].

	Ground State Atom	Metastable Atom
Initial Config.	$\rho_G = \rho_{Ge} \otimes \rho_{GN}$	$\rho_M = \rho_{Me} \otimes \rho_{MN}$
Hyperfine Inter.	ρ_G	$\rho'_M = \Sigma_F P_F \rho_M P_F$
		$= \rho'_{Me} \otimes \rho_{MN-\mathrm{Pol}}$
Metastab. Exch.	$\rho'_G = \rho_{Ge} \otimes \rho_{MN-\mathrm{Pol}}$	$\rho''_M = \rho'_{Me} \otimes \rho_{GN}$

1.3 Setup Overwiew

A pumping cell in which MEOP will be performed is to be located several meters away from EBIS. The magnetic field must be sufficiently uniform such that depolarization effects from transverse gradients are minimized. While it is possible to polarize in the strong kilogauss fringe fields with the aid of gradient correction coils, it is planned to instead construct cylindrical soft steel shielding inside which the pumping cell, Helmholtz coils, and polarization optics will be located. This provides maximum flexibility in the pumping cell location and allows polarization at low-field ($\sim$ 30 Gauss), where the MEOP process and our polarimetry methods are well-understood. A CAD drawing of the shielded Helmholtz pair is visible in Fig. (1-2), and a setup schematic in Fig. (1-3).

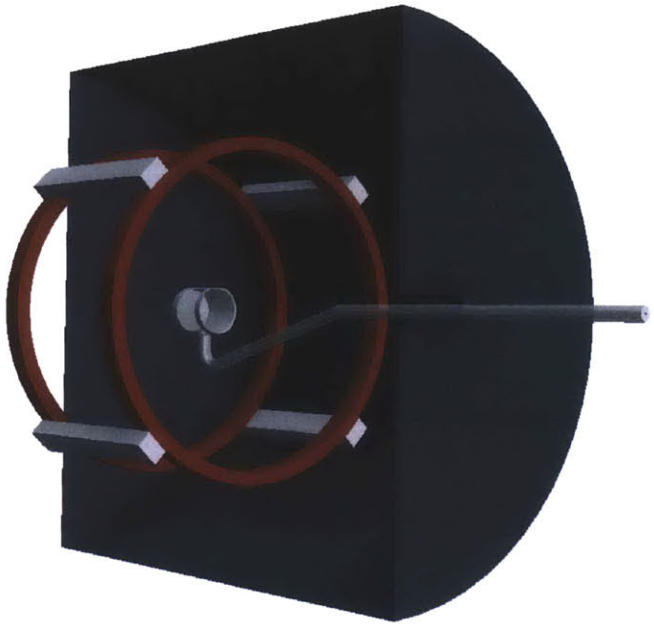

Figure 1-2: CAD drawing of shielded Helmholtz pair. (J. Maxwell)

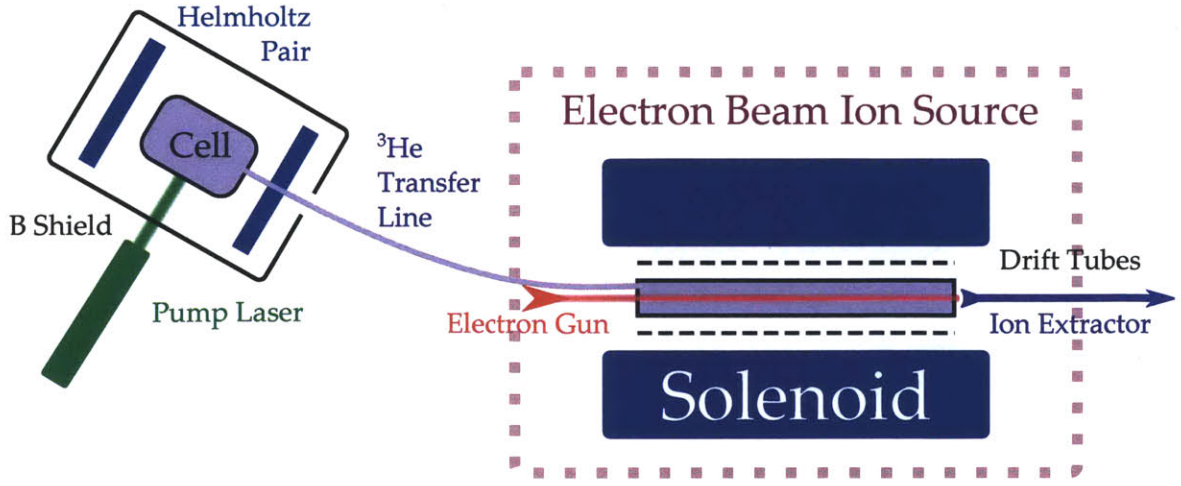

Figure 1-3: Overview of optical pumping setup near EBIS. (J. Maxwell)

Chapter 2

Optical Pumping using the Metastability Exchange Technique near EBIS

A number of technical constraints have been taken into account in the design of the EBIS-based polarized ion source. Often, these constraints lend a choice of technique for how they may be addressed. In many of the sections that follow, the various options and their parameters will be discussed, and the rationale for the choice will be presented.

2.1 EBIS Overview

As an successor to the Tandem Van de Graaff ion sources at RHIC, a more efficient Electron Beam Ion Source (EBIS) has been developed and was commissioned in 2010 [1]. The EBIS is a 1.5 meter-long ion trap with a 15 keV electron beam enclosed in a 5T superconducting solenoid (Figures 2-1, 2-2). Over the past several years, it has been used with great success to prepare a vast variety of highly-ionized species.

In order to extract approximately 10^{12} $^3He^{++}$ per second, it is intended to flow in roughly 3×10^{14} ^{3}He/sec.

2.1.1 EBIS Ion Trap Properties

In the following sections, the parameters for a number of properties of the EBIS ion trap are calculated. These include the operating pressure, ion trapping mechanisms, average time spent in the trap, and energy deposition by the electron beam.

Ionization in EBIS

In [12], Seltzer and Berger apply Bethe theory and Sternheimer density-effect corrections in order to estimate the collision stopping power of electrons through various materials. They arrive at:

$$-\frac{1}{\rho}\left(\frac{dE}{dx}\right) = \frac{0.153536}{\beta^2}\frac{Z}{A}B(T)$$

where $\beta = v/c$, Z is atomic number, A is atomic weight, and

$$B(T) = B_0(T) - 2\ln\left(\frac{I}{mc^2}\right) - \delta$$

where I is the mean excitation energy of the medium (41.8 eV for Helium), mc^2 is the rest energy of the electron (0.511 MeV), and δ is the density effect correction. Furthermore,

$$B_0(T) = \ln(\tau^2(\tau+2)/2) + [1 + \tau^2/8 - (2\tau+1)\ln 2]/(\tau+1)^2$$

where $\tau = T/mc^2$. T is the electron kinetic energy, which in EBIS is roughly 15 keV. Evaluating this yields $B_0(T) = -6.79$.

The density-effect correction, which accounts for the material becoming polarized as a charged particle traverses it, is estimated by a numerical formula piecewise in the parameter $X = \frac{1}{2}\log_{10}(\tau(\tau+2))$ [12]. Below a certain a material-specific X_0 value, $\delta = 0$. We find that this is the case for our parameters, where $X = -0.6125$ and for Helium, $X_0 = 2.191$. Thus, δ is indeed 0.

Thus, $B(T) = 12.0$ and therefore,

$$-\frac{1}{\rho}\left(\frac{dE}{dx}\right) = 21.9\ \frac{MeV}{g\ cm^{-2}}.$$

With $\rho = 10^{10}$ atoms$/cm^3 \rightarrow 4.98 \times 10^{-14}\ g/cm^3$,

$$-\frac{1}{\rho}\left(\frac{dE}{dx}\right) = 1.09 \times 10^{-12}\ MeV/cm.$$

As there are 6×10^{19} electrons passing over the length of EBIS (190 cm) each second, energy is deposited at a rate of $1.24 \times 10^{10}\ MeV/sec$. Since 79 eV are necessary to fully ionize a ^{3}He atom, an extraction rate of 3×10^{12} ions/sec requires about $2.4 \times 10^8\ MeV/sec$. Thus, the energy provided by the electron beam is sufficient by more than a factor of $\sim 10^2$.

Pressure Inside EBIS

In order to design the vacuum systems for providing ^{3}He flow to EBIS, the operating pressure must be estimated. Estimating that the EBIS turbopumps provide a vacuum outflow pumping speed of 100 l/s $= 10^5\ cm^3/s$ at the trap, then the pressure $P = Q/S$ [9] is

$$P = \frac{3 \times 10^{14}\ s^{-1}}{10^5\ cm^3 s^{-1}} = 3 \times 10^9\ cm^{-3} \rightarrow \sim 10^{-7}\ \text{torr}$$

Ion Trapping

Once the ^{3}He atoms become ionized in the electron beam, they are trapped by two main processes. For one, the positive ions are electrostatically attracted to the negatively-charged electron beam. Additionally, the positive ions are located in a strong 5T solenoidal magnetic field, and thus will undergo circular motion in the ρ, ϕ plane. The radius of curvature of their motion is given by

$$Bqv = \frac{mv^2}{r}.$$

With B = 5T, $q = 1.6 \times 10^{-19}\ C$, thermal velocity $v = 10^3\ m/s$, $m = 5 \times 10^{-27}\ kg$, it is calculated that $r \approx 6\ \mu m$. Along with the negative charge of the electron beam,

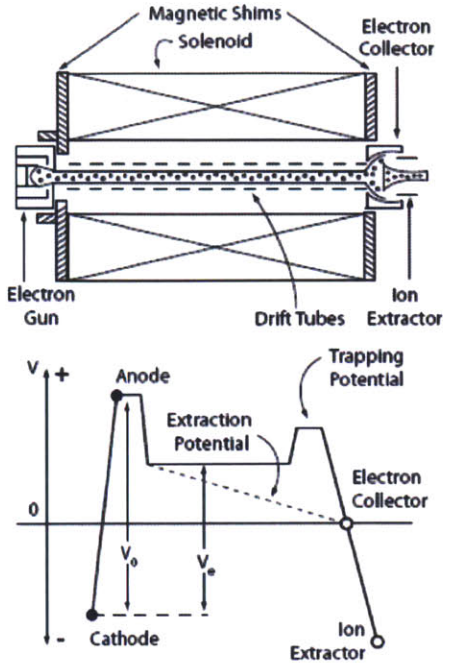

Figure 2-1: Top: a basic schematic of EBIS. Below: the electric potential along the length of EBIS. (A. Pikin)

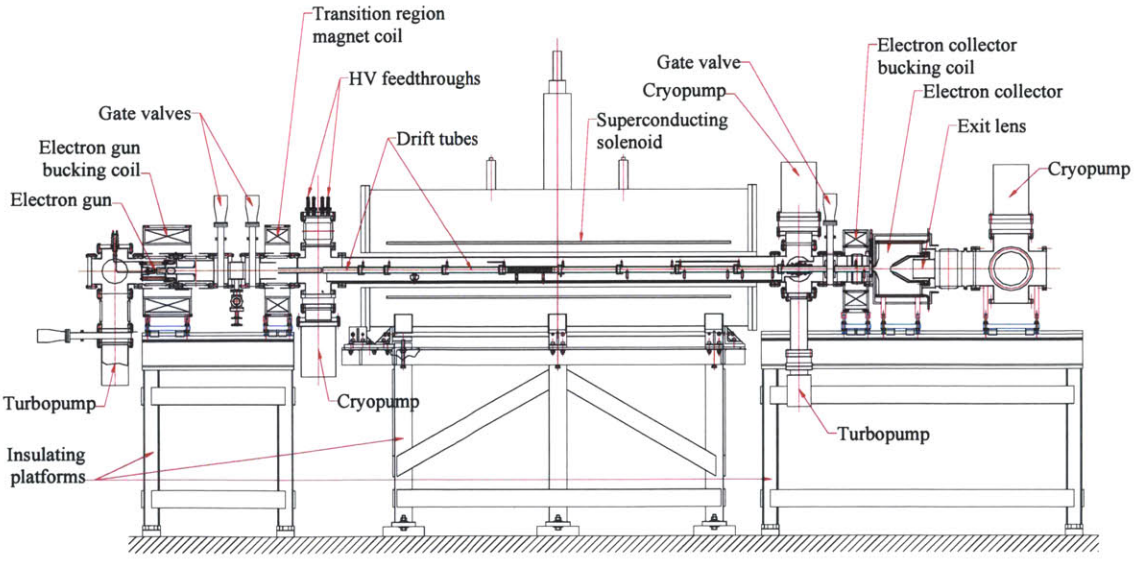

Figure 2-2: A schematic of EBIS. (A. Pikin)

this means that the $^3He^{++}$ ions are confined to the trap once ionized. Significantly, this implies that they will not later undergo wall bounces.

Time Spent in Trap

Another important figure is the approximate time spent in the trap, which is important as a figure of reference for polarization relaxation processes. First, the equilibrium number of atoms in the trap is estimated. With a trap length of 1.5 m and an approximate diameter of 5 cm, the volume of gas in the trap is

$$\frac{25\pi}{4} \cdot 150\ cm^3 = 2945\ cm^3 \approx 3,000\ cm^3.$$

Then this implies that there are

$$3 \times 10^9\ cm^{-3} \cdot 3 \times 10^3\ cm^3 =$$

$= 9{\times}10^{12}$ atoms inside EBIS at equilibrium. Then, comparing this with the extraction rate, the average time the atoms spend in the trap is

$$\frac{9 \times 10^{12}}{3 \times 10^{14}\ s^{-1}}\ s \approx 30\ ms.$$

So far, all discovered relaxation processes seem to occur over far longer time scales.

2.1.2 Flow from the Pumping Cell to EBIS

Polarized ^3He atoms must be transferred from the pumping cell at $P_0 \approx 1$ torr to EBIS at $\sim 10^{-7}$ torr. It is calculated that the flow conductance between the pumping cell and EBIS must be approximately $8 \times 10^{-6}\ l/s$, based on principles outlined in [9]. A calibrated capillary leak at 10^{-5} atm-cc/sec at the pumping cell and a $O(mm)$ diameter tube to EBIS will provide the necessary flow rate. The transfer line should be made of glass so that it can withstand high vacuum and so that it can be baked to minimize outgassing.

2.2 Possible Processes In EBIS Leading to Depolarization

There are a number of processes that take place inside EBIS that may lead to depolarization. They include:

- Charge exchange. $^3He^+ + {}^3He^{++} \rightarrow {}^3He^{++} + {}^3He^+$

  This has a cross section of $\sigma \approx 10^{-16}\ cm^2$, and is thus thought to occur at a very low rate.

- Recombination. $^3He^+ + e \rightarrow {}^3He$; $^3He^{++} + e \rightarrow {}^3He^+$

  This is a 3-body process and thus thought to be unlikely. The cross section is lowered by a factor of α^2, thus $\sigma < 10^{-20}\ cm^2$

- Spin-exchange collisions. These are thought to occur at a low rate. The cross section for neutral Hydrogen spin-exchange collisions is approximately $10^{-14}\ cm^2$; for ^3He ions it is expected to be even lower. It is expected that due to coulomb interactions, the ions will not even approach close enough for spin-exchange to occur.

- Wall depolarization of atoms inside EBIS. This is thought to be low because of the low probability of depolarization in a wall collision. Further study is underway to understand how many atoms will collide with the walls before being ionized.

2.2.1 A Note on Charge Exchange

It is important to investigate charge exchange because $^3He^+$ has a free electron which can depolarize, and then cause the nucleus to depolarize via hyperfine coupling. If a $^3He^+$ and a $^3He^{++}$ ion undergo charge exchange, depolarization in the $^3He^+$ population can propagate to the $^3He^{++}$ ions.

We approximate the rate of charge exchange as $\rho_1\rho_2\bar{v}\sigma V$, where ρ_1, ρ_2 are the densities of singly and doubly ionized ^3He, $\bar{v}$ is the average velocity, $\sigma = 10^{-16}\ cm^2$ is

the charge exchange cross section, and V is the volume. We approximate the densities as both being $3 \times 10^7\ cm^{-3}$, which corresponds to 1% of the gas being ionized. Then the rate is

$$\begin{aligned}(3 \times 10^7\ cm^{-3})(3 \times 10^7\ cm^{-3}) \cdot 10^5\ cm\ s^{-1} \\ \times 10^{-16}\ cm^{-2} \cdot 3 \times 10^3\ cm^3 \\ = 2.7 \times 10^7\ s^{-1} \\ \approx 3 \times 10^7\ s^{-1}\end{aligned}$$

Since the rate of ion extraction is approximately $10^{12}\ s^{-1}$, it is thought that even if singly-charged ions depolarize and undergo charge exchange, the effects will be minimal.

2.2.2 Wall Bounces in Transfer Line

In [15], the relaxation time of ^{3}He was measured on various surfaces. In an enclosed space with surface area A, such as the pumping cell, the number of wall collisions per unit time is given by $\frac{1}{4}\rho\bar{v}A$, where ρ is the density and $\bar{v}$ is the average velocity. With a measured relaxation time T, the probability to depolarize per collision is approximately

$$P \approx \frac{1}{T\frac{1}{4}\rho\bar{v}A} \approx 10^{-20}$$

In a glass transfer line with an average number of collisions of 10^6, the expected depolarization is 1 part in 10^{14}, which is negligibly small.

2.3 Magnetic Field Gradients

A strong transverse magnetic field gradient can cause depolarization if the field direction in the particle's rest frame appears to oscillate near the Larmor frequency [10]. The polarization relaxation time of the ^{3}He is related to the strength of the transverse magnetic field gradients by the equation [10]:

$$\frac{1}{\tau} = \frac{2}{3}\frac{|\Delta B_t|^2}{|B_l|^2}\langle v^2\rangle \frac{\tau_c}{\omega_0^2\tau_c^2 + 1} \tag{2.1}$$

where for ^{3}He, $\omega_0 = 3.24\ |B_l|\ kHz/Gauss$ and $\tau_c \approx 2.2 \times 10^{-7} p^{-1}$, where p is in torr.

Such magnetic field gradient effects should be the dominant depolarization process in the transfer line. The polarization decays exponentially as $\exp(-t/\tau)$, thus for a transfer line with τ a function of position, this can be generalized to

$$P = P_0 \exp\left(-\sum_i \frac{\Delta t_i}{\tau_i}\right). \tag{2.2}$$

for a particle spending time Δt_i at each location i. Assuming the transfer velocity is reasonably constant, we can factor out the Δt_i into the total transfer time Γ and number of locations N; thus

$$P = P_0 \exp\left(-\frac{\Gamma}{N}\sum_i \frac{1}{\tau_i}\right). \tag{2.3}$$

The relaxation time τ_i is calculated at each point on the proposed path, and then Eq. (2.3) is computed. As an estimate, the transfer line is chosen to begin at (-110 cm, 70 cm), move to (-110 cm, 10 cm), then into EBIS at (-80 cm, 10 cm), the coordinate origin being the center of the trap, as in Fig. (2-3). With the short transfer times associated with molecular flow (10^{-3} seconds), the polarization retention along this sample path is calculated to be greater than 98%.

Since the gradient of the magnetic field is represented by a tensor, the transverse gradient (to the holding field) observed by the atom is dependent on its path. In

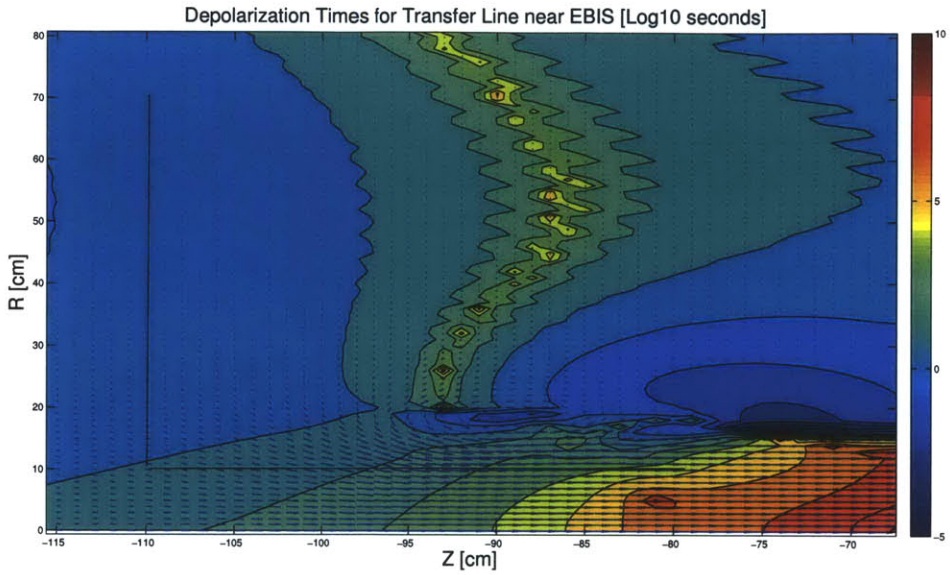

Figure 2-3: Simulated transfer line location in EBIS field

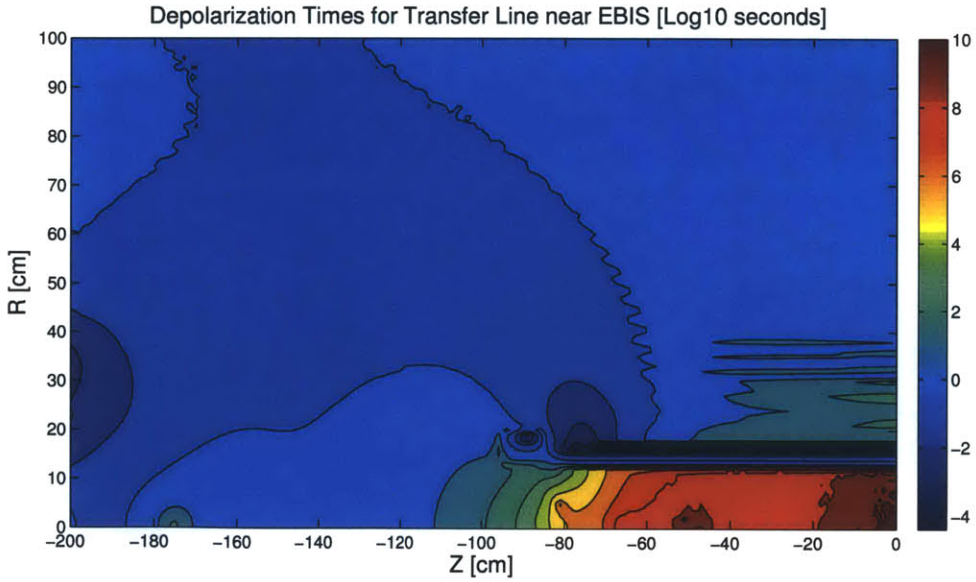

Figure 2-4: Heat-map showing polarization relaxation times near EBIS solenoid (center at origin).

some cases, aligning the path of the atoms with a field line can produce a desirable reduction in the transverse gradient. However, the extent of the improvement depends greatly on the specific field configuration: in some instances, there is little benefit to following a field line, and in others, it is significant. As the atoms are bouncing along the interior of the transfer line, the direction of the velocity vector is changing rapidly, and thus in calculations, it is sometimes difficult to pin down the precise choice of "which" transverse gradient is applicable. Our interpretation of [10] leads us to believe that the chaotic motion of the atoms necessitates that the transverse gradients in all three dimensions should be added in quadrature in the squared term of Eq. (2.1).

Chapter 3

Experimental Realization

3.1 MIT Campus Lab

A lab on the MIT campus has been established for the development of the ion source. Tests have been performed on sealed ^{3}He cells in order to understand and optimize the polarization process. Two Keopsys 10W "HePup" fiber lasers provide 1083 nm light for optical pumping of the C_8 or C_9 transitions. Light emerges from the fiber head in a linearly polarized state, which is then passed through a polarizing beam-splitting cube, a quarter-wave plate, and then beam expansion optics. After passing through the cell, a mirror reflects the transmitted laser light back through the cell for a second pass. The light continues back through the laser optics and upon reaching the quarter-wave plate becomes rotated in polarization relative to the original beam; thus, when passing through the polarizing beam-splitting cube (PBS), it is deflected into a Thorlabs DET36A silicon photodiode rather than the laser head. This allows a continuous measurement of absorption to be performed. Fig (3-1) shows a diagram of the setup. Data is acquired with a National Instruments PXIe-1078 DAQ crate, with a PXIe-6363 X Series Multifunction DAQ card connecting to two remote BNC connector pods (BNC-2110 and BNC-2111), and a PXIe-8370 MXI Express interface connecting to a PCIe slot on the lab computer. The DAQ system interfaces directly with LabView, in which routines are programmed. USB/serial connections interface with the controllers for Thorlabs SH1 shutters, the controllers for Thorlabs LCC1112-

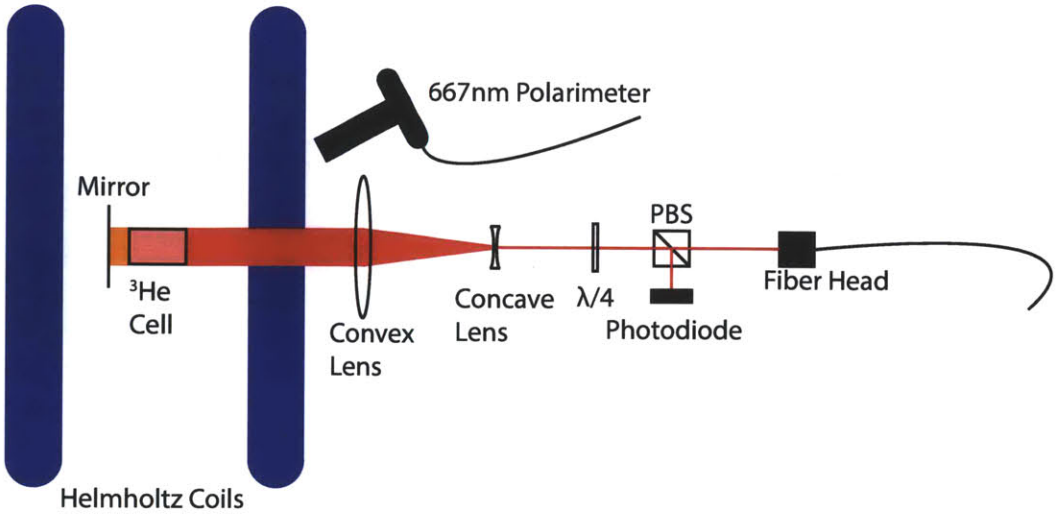

Figure 3-1: Diagram of the MIT lab setup.

B and LCC1111-C liquid crystal retarders, and a TTL control of the RF discharge, enabling nearly complete hardware automation.

3.1.1 Keopsys Lasers

The Keopsys 1083 nm ytterbium fiber lasers are manufactured for the purpose of ^{3}He optical pumping, and can be operated at a power level of up to 10W. After a brief warm-up period ($\sim$ 10 minutes), the laser is tuned to either the C_8 or C_9 transition by absorption spectroscopy on a secondary ^{3}He discharge cell. A secondary laser monitor fiber output is used for this so that the polarization setup is not disturbed and so that the calibration can be performed continuously. An infrared-optimized photomultiplier tube is positioned perpendicular to the monitor fiber output so that the re-radiated infrared light can be detected: at resonance, the light is reradiated primarily at ninety degrees. The transitions can be mapped this way by observing a strong signal when the laser is tuned to resonance.

The laser can be tuned either by a potentiometer on the device or by a ramp voltage input. The latter method has been used with a LabView-generated DC ramp in order to map the ^{3}He transitions at 1083 nm. The laser assigns a tune value based on the setting indicated by the potentiometer or input ramp voltage; however, this was seen to be unreliable day-to-day in predicting the precise output wavelength.

Combined with a slight drift in frequency during operation, this necessitated frequent and constant calibration. As the tuning cell absorption measurement can be made continuously and the wavelength can be controlled externally, a future revision of our data acquisition software will include a PID loop to follow the resonance and automatically keep the laser tuned.

3.1.2 Polarimetry

Several methods can be used to measure the ^{3}He nuclear polarization. NMR is a natural approach, but the coupling of nuclear and electronic spins can be harnessed to provide a simpler and more efficient polarization measurement. While the weak RF discharge is activated, various spectral lines can be analyzed in order to indirectly learn the nuclear polarization state. The two primary methods for polarization measurement involve infrared probe absorption, or optical polarimetry of the 667nm discharge line.

Performing the pump-probe polarimetry measurement is conceptually simple. A circularly polarized probe laser is directed transverse to the pumping cell. This circularly polarized light consists effectively of two linearly polarized components, one that is transverse to the polarization axis, and one that is along it. The ratio of the transmitted power of transverse to longitudinally polarized light is calculated, giving the ratio of populations in the two 2^3S sublevels [14]. The population densities are known as a function of polarization, and thus the nuclear polarization can be inferred [14].

A legacy polarimeter from previous MIT internal target tests has been explored as a first polarimetry option. This type of polarimeter indirectly measures the nuclear polarization by observing the circular polarization of the 667 nm discharge line. The calibration between optical and nuclear polarizations was performed in [6]. Light first passes through a rotating quarter-wave plate, which transforms the circularly polarized light into a rotating linearly polarized wave. This passes through a linear analyzer, which converts it to a wave of oscillating amplitude. The light passes through a 667 nm bandpass filter and is then detected by a photomultiplier tube. A

chopper on the rotating waveplate mount provides a reference signal by which a lock-in amplifier can measure the AC amplitude of the signal. A DC amplifier magnifies the constant level of the signal, and the ratio of the AC to DC components provides the optical polarization. There exists a correction factor of $1/\cos(\theta)$, where θ is the angle between the polarimeter and the polarization axis, that must also be applied to compensate for observing the circularly polarized light from a nonzero angle of incidence [11].

A new generation of 667 nm polarimetry is being developed using a liquid crystal retarder and photodiode to replace, respectively, the rotating quarter-wave plate and photomultiplier tube. The liquid crystal retarder is set to oscillate between the $\lambda/4$ and the $3\lambda/4$ states, producing transmitted intensities I_1 and I_2, lending an optical polarization of $P = (I_1 - I_2)/(I_1 + I_2)$. This method has higher statistical uncertainty than the legacy method, as the signal being measured is at 1 Hz rather than at the high waveplate rotation frequency ($\sim$200 Hz), but the much greater simplicity lends to a strong reduction in potential systematic offsets. A Thorlabs PDF10A femtowatt photoreceiver is sufficiently sensitive to provide the necessary precision in the polarization measurement (variation of less than 1%). When a circularly polarizing filter is placed before the polarimeter (to simulate measuring 100% polarization), the signal-to-noise as the liquid crystal retarder changes states is quite large. This can be seen in Fig. (3-2). When this optical polarimetry technique is used, the room lights are switched off and a sodium lamp is turned on, so that there is no ambient 667nm light that could interfere with the measurement.

3.2 Sealed Cell Production at Bates

Sealed cells for initial polarization tests have been produced at MIT-Bates. A sealed cell consists of two optically-clear windows (fused silica or #7740 Pyrex) of 2-inch diameter, connected by a 2-inch length #7740 Pyrex cylinder. The empty cells, custom manufactured by Finkenbeiner, Inc., of Waltham, MA, are initially produced with a glass to mini-conflat extension piece for attachment to filling equipment. Alternating

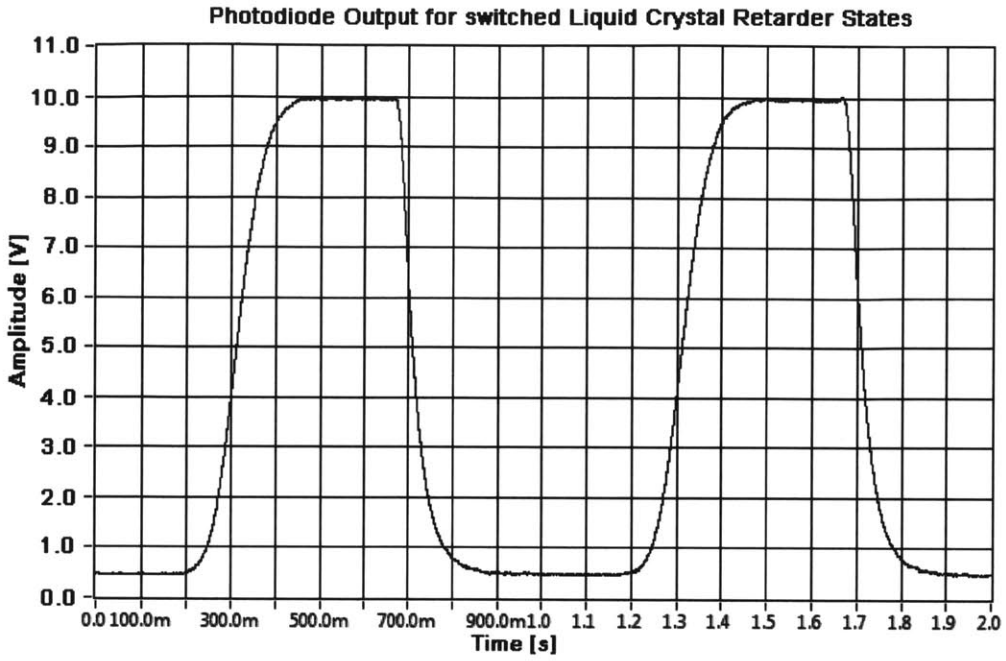

Figure 3-2: Plot showing the PDF10A femtowatt photoreceiver output (volts) as the liquid crystal retarder changes states, with a circularly polarizing filter engaged.

cycles of baking and running of a strong RF discharge are used to clean the cell prior to filling. A residual gas analyzer is used to verify the removal of water vapor and other unwanted gases, and the spectral lines of the discharge are analyzed in order to verify purity. When finished, the cell is flamed off from the system. A schematic of the setup is visible in Fig. (3-4).

3.3 Preliminary Polarization

Polarization of a new sealed cell has been achieved and measured with the liquid crystal retarder technique. Fig. (4.4) shows a plot of the polarization versus time as the laser is first turned on and then off. This shows a preliminary achievement of approximately 40% nuclear polarization, with the quite satisfactory pump-up and discharge-on relaxation times of 4.9 ± 0.4 s and 38.3 ± 0.5 s, respectively. An increase of the polarization level is expected with further study and optimization.

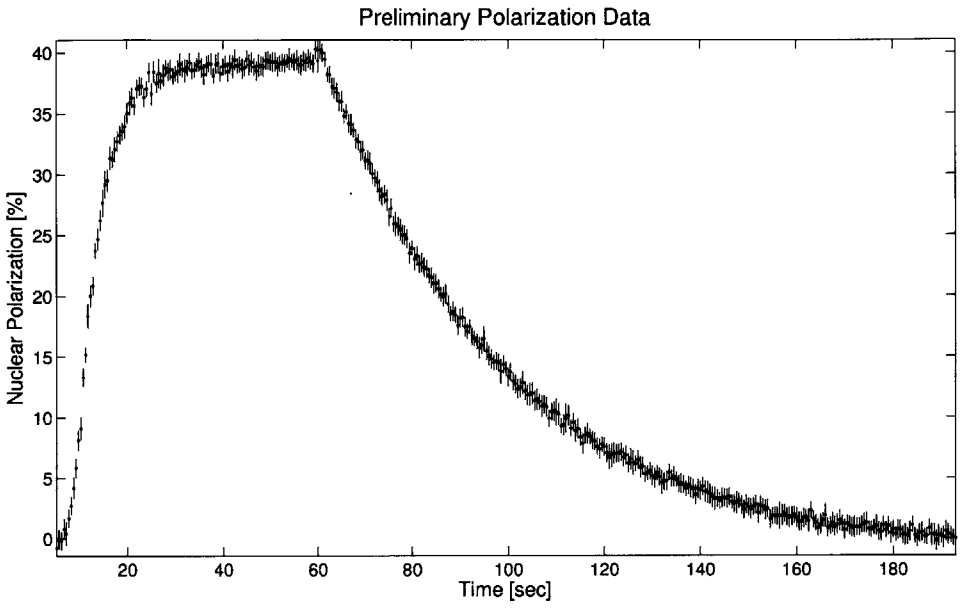

Figure 3-3: Plot of polarization versus time for new sealed cell, measured with liquid crystal retarder.

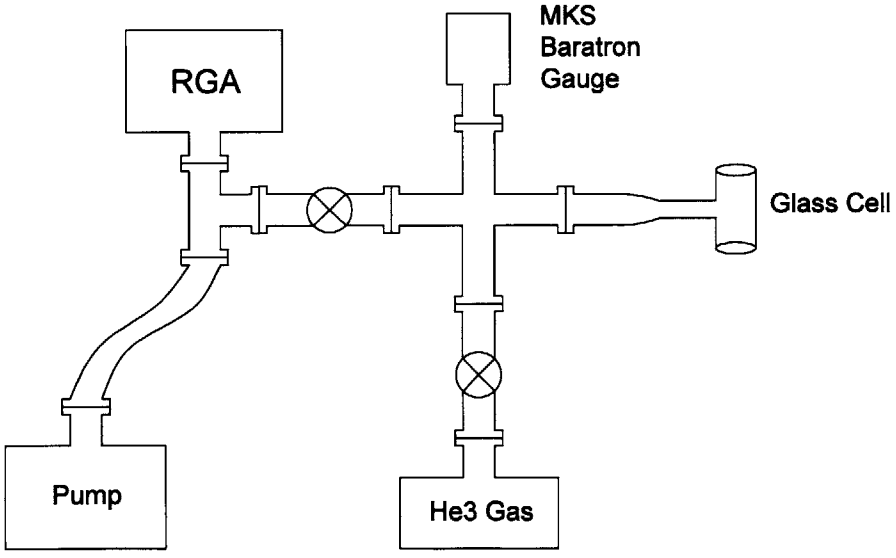

Figure 3-4: Sealed cell production system schematic

Chapter 4

Test of Source Concept at RHIC

In order for the polarized ion source to be viable as planned, the polarized ^{3}He atoms must retain their polarization in transit to EBIS. Theoretical predictions indicate the feasibility of this transfer. A test experiment, planned for the summer of 2013, is being designed to provide experimental verification.

^{3}He atoms will be polarized in a shielded pumping cell, and then transferred to a secondary cell inside the EBIS solenoid. In the secondary cell the polarization can be measured with a modified IR probe technique. Additionally, the polarization in the second cell can be inferred by measuring its effects on the polarization of the first cell. A schematic of the setup is visible in Fig. (1-3), and a CAD drawing in Fig. (4-2).

4.1 Polarization Measurement with a Two-Cell System

A two-cell system for measuring the polarization retention in transit to EBIS involves optically pumping ^{3}He atoms in a pumping cell far from EBIS, allowing them to diffuse into a second cell within the EBIS solenoid, and inferring the polarization in the second cell from that of the first. The polarization in the second cell can be inferred by killing the polarization in the pumping cell and measuring the inflow of

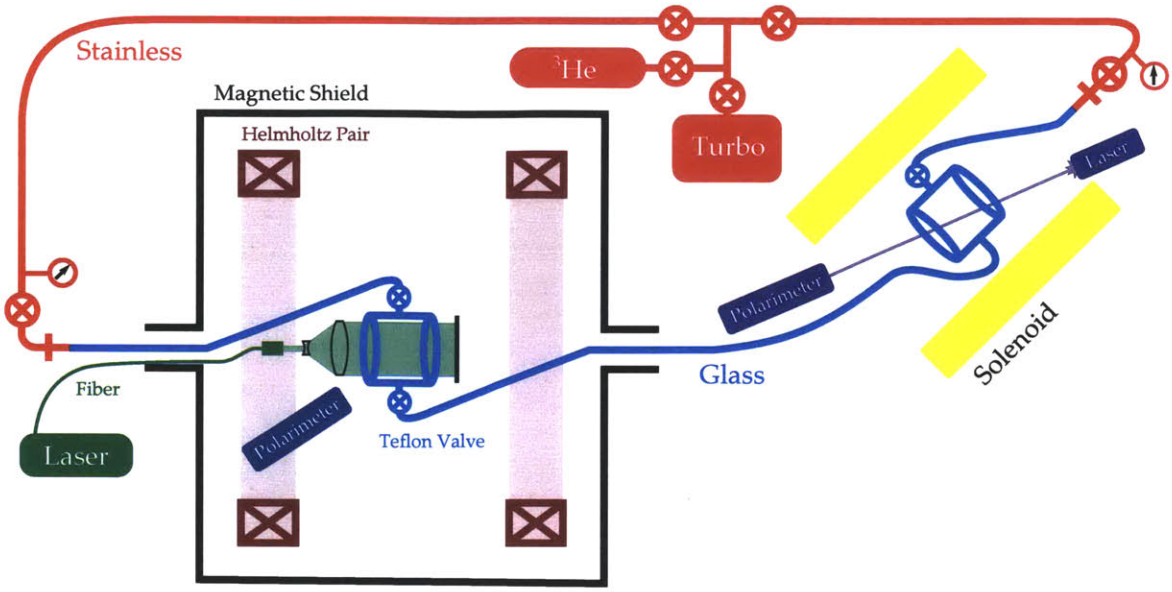

Figure 4-1: Test experiment setup schematic. (J. Maxwell)

polarized atoms. This method is explained in detail in [5].

4.1.1 Equilibrium Polarization Measurement

An alternative, simple, method for making a measurement of the polarization retention is to observe the change in equilibrium pumping cell polarization when the transfer line to the second cell is opened. The mechanics of such a measurement are described.

Based upon those in [5, 7], the rate equations for a two-cell system can be described as:

$$\dot{P}_p(t) = -\frac{P_p(t)}{\tau_p} - \frac{P_p(t)}{T} + \frac{DP_t(t)}{T} + P(1 - P_p(t)) \tag{4.1}$$

$$\dot{P}_t(t) = -\frac{P_t(t)}{\tau_t} - \frac{P_t(t)}{T} + \frac{DP_p(t)}{T} \tag{4.2}$$

where $P_p(t)$ is the polarization in the pumping cell, $P_t(t)$ the test (EBIS) cell polarization, τ_p and τ_t the relaxation times in the respective cells, T the "communication time" between cells, D the fraction of polarization retained in transit, and P the

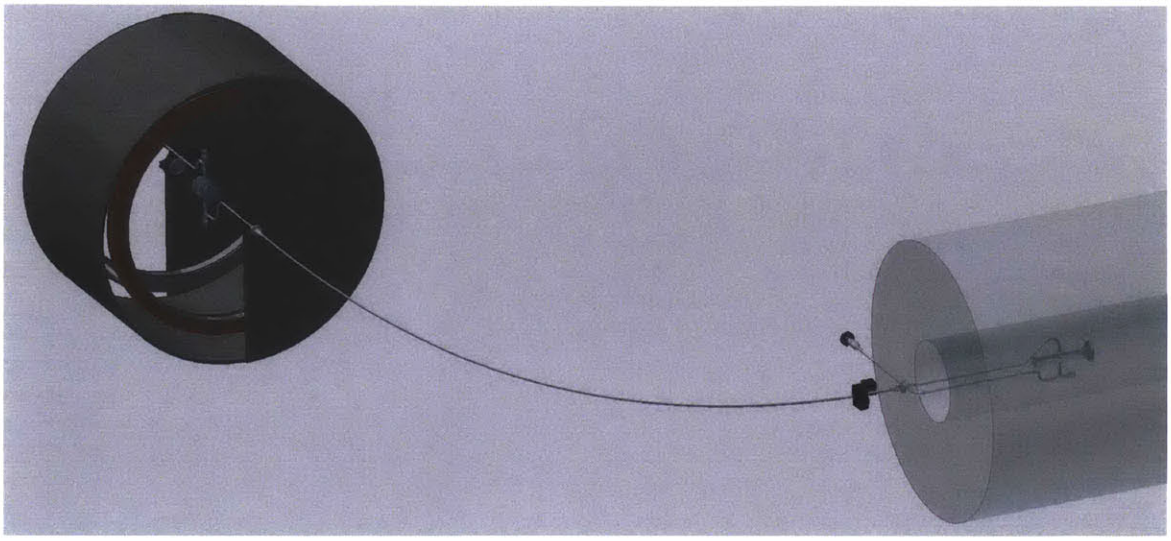

Figure 4-2: Cutaway CAD drawing of test setup. (J. Maxwell)

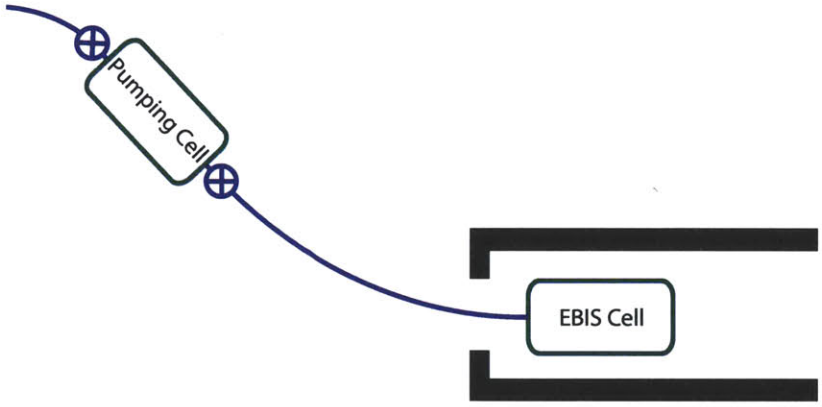

Figure 4-3: Schematic of Two-Cell Setup

pump rate. The first term in each line represents relaxation within the respective cell, the second term reflects polarized ^{3}He atoms flowing out of the cell, and the third term, polarized ^{3}He flow into the cell. The final term in (4.1) reflects the ongoing polarization by optical pumping.

Assuming that there is negligible relaxation in EBIS at 5T, let $\tau_t \to \infty$. Then at steady state, Eq. (4.2) indicates

$$P_t = DP_p, \tag{4.3}$$

and thus (4.1) becomes

$$-\frac{P_p}{\tau} - \frac{P_p}{T} + \frac{D^2 P_p}{T} + P(1 - P_p) = 0.$$

Solving, we find:

$$P_p = \frac{P}{\frac{1}{\tau} + \frac{1-D^2}{T} + P}. \tag{4.4}$$

To estimate the change in equilibrium polarization when the transfer line is opened, we first solve for P in the single-cell system. Examining only the pumping cell by dropping the transfer terms (i.e., letting $D = 1$), we find that if 50% polarzation is reached in the pumping cell (i.e., $P_p = 0.5$), and $\tau = 10\ s$, that $P = 0.1$. When the transfer line is opened, using this value of P and a transfer time of $T = 8.7\ s$, we examine the equilibrium polarization as D ranges from 0 to 1. With full polarization retention in the transfer, the equilibrium polarization remains 50%; with full loss, it is approximately 32%.

4.1.2 Sensitivity of EBIS Cell Polarization Measurement

Rearranging Eq. (4.4), it follows that:

$$D = \left[1 + \frac{T}{\tau} + PT\left(1 - \frac{1}{P_p}\right)\right]^{\frac{1}{2}}. \tag{4.5}$$

If the error in measuring D is dominated by the measurement error of P_p, then at $D = 1$, the error introduced is $\delta D \approx 1.74 \delta P_p$. As $D \to 0$, the error increases without bound; at $D = 0.4$ it is roughly a factor of 10.

Propagating error from Eq. (4.3), it follows that

$$\delta P_t = \sqrt{(D\delta P_p)^2 + (P_p \delta D)^2} \tag{4.6}$$

Estimating $\delta P_p = 0.03$ and using the above parameters, we find at $D = 0.4$, $\delta P_t \approx 0.1$ and at $D = 1$, $\delta P_t \approx 0.04$. Thus, if the pumping cell polarization can be measured to $\pm 3\%$ accuracy, the EBIS cell polarization should be known to within $\pm$4-10% if

the polarization retention is above 40%. Estimating ballpark errors on the other parameters to be $\delta f = 0.05$, $\delta P = 0.005$, $\delta\tau = 0.2\ s$, $\delta T = 1\ s$, the expected error δP_t rises to ±4-12%.

4.1.3 Expected Polarization Retention in Transfer

Earlier, the polarization retention in a molecular flow transfer line was calculated to be greater than 98%. However, at a higher pressure in this configuration of 1 torr, the flow will not be molecular. While the "communication time" for polarization to equalize between the two cells is expected to be on the order of ~ 8.7 seconds (which would completely depolarize the atoms), the transfer time for any *individual* atom to flow through the transfer line at 1 torr is hoped to be small. This will be tested, and if necessary, a measurement method that avoids this complication will be developed.

4.2 Summary

Development is underway for providing a source of highly-polarized ^{3}He ions to RHIC using metastability exchange optical pumping and the Electron Beam Ion Source. This will provide the world's first high-energy polarized neutron beam in a collider, a remarkable asset to studies of nuclear spin structure. Realization of the source at an MIT campus lab is ongoing, and a test of the concept is being prepared for summer 2013.

Bibliography

[1] Electron beam ion source. `http://www.bnl.gov/cad/ebis/`, August 2010.

[2] W. E. Burcham, O. Karban, S. Oh, and W. B. Powell. A source of polarized 3he ions. *Nuclear Instruments and Methods*, 116(1):1–7, March 1974.

[3] Jacques Dupont-Roc, Michele Leduc, and Franck Laloe. New value for the metastability exchange cross section in helium. *Phys Rev Lett*, 27(8), 1971.

[4] D. O. Findley, S. D. Baker, E. B. Carter, and N. D. Stockwell. A polarized 3he+ ion source. *Nuclear Instruments and Methods*, 71(2):125–132, June 1969.

[5] C. E. Jones et al. $^3He(e,e')$ *Quasielastic Asymmetry. Phys. Rev. C*, 47, 1993.

[6] W. Lorenzon et al. Nmr calibration of optical measurement of nuclear polarization in 3he. *Phys. Rev. A*, 47(468), 1993.

[7] J. D. Maxwell. Gas-transfer depolarization test for a polarized ^{3}he ion source at rhic. 2012.

[8] RG Milner. "Development of a Polarized ^{3}He Ion Source for RHIC," funded by the Office of Nuclear Physics Program for R&D for Next Generation Nuclear Physics Accelerator Facilities, 2010.

[9] Alexander Roth. *Vacuum Technology.* North Holland, 1982.

[10] L. D. Schearer and G. K. Walters. Nuclear spin-lattice relaxation in the presence of magnetic-field gradients. *Phys. Rev.*, 139(5A):A1398–A1402, Aug 1965.

[11] Dirk De Schepper. *Spin-dependent deep inelastic positron scattering from a polarized helium-3 internal gas target.* PhD thesis, Massachusetts Institute of Technology, 1997.

[12] Stephen M. Seltzer and Martin J. Berger. Evaluation of the collision stopping power of elements and compounds for electrons and positrons. *The International Journal of Applied Radiation and Isotopes*, 33(11):1189 – 1218, 1982.

[13] R. J. Slobodrian. New method for the production of polarized 3He ions based on the 23S1 state of 3He. *Nuclear Instruments and Methods in Physics Research*, 185(1-3):581–583, June 1981.

[14] C. Talbot, M. Batz, P. J. Nacher, and G. Tastevin. An accurate optical technique for measuring the nuclear polarisation of 3He gas. *Journal of Physics: Conference Series*, 294, 2011.

[15] R. S. Timsit, J. M. Daniels, and A. D. May. Nuclear relaxation of ^{3}He gas on various solid surfaces. *Canadian Journal of Physics*, 49(560), 1971.